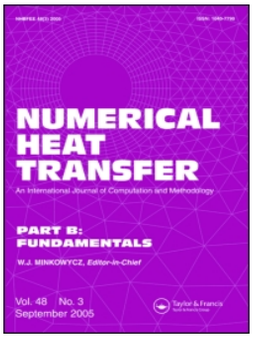

Taylor & Francis
Taylor & Francis Group

Numerical Heat Transfer, Part B: Fundamentals
An International Journal of Computation and Methodology

ISSN: 1040-7790 (Print) 1521-0626 (Online) Journal homepage: http://www.tandfonline.com/loi/unhb20

A parallel scalable multigrid method and HOC scheme for anisotropy elliptic problems

Zhao-Hui Li, Lei Chen & Wen-Quan Tao

To cite this article: Zhao-Hui Li, Lei Chen & Wen-Quan Tao (2017) A parallel scalable multigrid method and HOC scheme for anisotropy elliptic problems, Numerical Heat Transfer, Part B: Fundamentals, 71:4, 346-358, DOI: 10.1080/10407790.2017.1293959

To link to this article: https://doi.org/10.1080/10407790.2017.1293959

Published online: 05 Apr 2017.

NUMERICAL HEAT TRANSFER, PART B
2017, VOL. 71, NO. 4, 346–358
http://dx.doi.org/10.1080/10407790.2017.1293959

Taylor & Francis
Taylor & Francis Group

A parallel scalable multigrid method and HOC scheme for anisotropy elliptic problems

Zhao-Hui Li, Lei Chen, and Wen-Quan Tao

Key Laboratory of Thermo-Fluid Science and Engineering of MOE, School of Energy and Power Engineering, Xi'an Jiaotong University, Xi'an, China

ABSTRACT
Anisotropy problems are widely encountered in practical applications. In the present paper, a parallel and scalable multigrid (MG) method combined with the high-order compact difference scheme is employed to solve an anisotropy model equation on a rectangular domain. The present method is compared with the MG combined with the standard central difference scheme. Numerical results show that the MG method combined with the high-order compact difference scheme is more accurate and efficient than the MG with the standard central difference scheme for solving anisotropy elliptic problems. MG components (restriction, prolongation, relaxation, and cycling) and the corresponding parallelism characteristics are also discussed.

ARTICLE HISTORY
Received 6 September 2016
Accepted 20 January 2017

1. Introduction

Numerical solution of anisotropy elliptic diffusion problems is frequently encountered in computational fluid dynamics. In the view of the discretization process, the sources of the anisotropy discrete algebraic equation step from two aspects: varying coefficients and grid stretching. First, the anisotropy term describes the properties of materials of being directionally dependent [1]. Heat conduction, for example, is anisotropy in the cases of fiber-reinforced composites. The longitudinal thermal conductivity of the unidirectional carbon fiber-reinforced plastic with a fiber volume fraction of 60% can be greater than that in transverse direction by 50 times [2]. Second, uniform grids discretization is inappropriate for many physical problems involving boundary layers. To get an accurate solution on a limited number of grids, grid points are clustered inside the boundary layers which are featured by large gradients [3,4]. As a result, the nonuniform distributions of grids also introduce anisotropy in a discrete algebraic equation. In recent years, a number of studies about anisotropy elliptic diffusion problem have been published. Wang et al. [5] proposed a new combined procedure IEFEM (radiative integral equation and finite element method) for solving radiative heat transfer in anisotropic scattering media. This new IEFEM scheme has prefer to geometry adaptability and can predict the anisotropy radative heat transfer accurately. To remove angular false sacttering, Hunter and Guo [6] implemented four higher-order quadrature sets for calculation of radiative transfer in a three-dimensional cubic enclosure containing participating media. A proper phase-function normalization is implemented to efficiently obtain accurate results. Tsai et al. [7] adopted a coordinate transformation (CT) method to investigate the microscale anisotropic thin-film heat conduction surrounded by an ultrafast pulse laser heating. Three different models are used to study the influence of thermal properties on the anisotropic heat

CONTACT Wen-Quan Tao wqtao@mail.xjtu.edu.cn Key Laboratory of Thermo-Fluid Science and Engineering, Ministry of Education, School of Energy and Power Engineering, Xi'an, Shaanxi, People's Republic of China.
Color versions of one or more of the figures in the article can be found online at www.tandfonline.com/unhb.

Nomenclature

a_{nb}	coefficients of the neighbor grid points
a_p	coefficient of the master grid point
e	absolute maximum errors
E_p	parallel efficiency
M	convergence rate
n	grid number
r	residual at fine grid point
R	residual at coarse grid point
s	source function
S_p	speed up
v	grid volume at fine grid point
V	grid volume at coarse grid point
δ	difference operator
ε	constant
Φ	solution variable
η	constants
λ	grid stretching parameter

Subscripts

i,j,k	number index
x, y, z	coordinate variables

conduction. Guedri et al. [8] compared FTn finite volume method (FTn FVM) with standard FVM for transient radiative transfer in anisotropically scattering medium. It is found that FTn FVM can largely reduce the ray effects and obtain more accurate results than standard FVM. Also, using the same spatial discretization scheme, FTn FVM has higher convergence rate than the standard FVM [8]. More recently, Liu et al. [9] derived a direct numerical finite volume scheme for anisotropic diffusion problems on skewd meshes. Compared with balance-point method and adaptive method, the direct method has the least convergence time [9].

High-order compact (HOC) schemes in combination with a variety of solution strategies have drawn much attention in international computational community in the past two decades [10–15]. Following is a brief review for papers published since 2000. Gupta and Zhang [10] presented a multigrid solving strategies of 3D convection–diffusion equation approximated by a fourth-order HOC scheme. Zhang et al. [11] poposed a new fourth-order 15 points HOC difference scheme for the 3D convection–diffusion equation. In [11], Zhang et al. adopted a parallelization mulitigrid (MG) method to accelarate solution process. Wang and Zhang [12] developed a sixth-order HOC solution procedure to solve 2D poisson equation. The studies mentioned above [10–12] are all based on uniform mesh size discretization. A transformation-free HOC scheme on nonuniform grids for a steady 2D convection–diffusion equation has been studied by Kalita et al. [13]. And then Ge and Cao [14] introduced a MG method based on [13] to accelerate the solution process. Prieto et al. [15] compared two robust multigrid methods for anisotropy elliptic equations. But the accuracy of the discretization operator they adopted is only second order.

In this paper, HOC difference schemes are adopted to solve anisotropy diffusion equations with the advantages of high accuracy and compact scheme stencils for nonuniform grid network. A parallel scalable MG method is developed to solve the resulting sparse linear equations, and the numerical properties are discussed.

The rest of the paper is organized as follows: In Section 2, a mathematical model of anisotropy problems and HOC difference scheme are described. In Section 3, a parallel scalable MG algorithm combined with HOC is presented. The simulation results are presented in Section 4, and finally, some conclusions are given in Section 5.

2. Mathematical model and HOC discretization

A 3D anisotropy diffusion equation with Dirichlet boundary condition studied in this paper is given by the following equations:

$$\varepsilon\frac{\partial^2\phi}{\partial y^2}+\left(\frac{\partial^2\phi}{\partial x^2}+\frac{\partial^2\phi}{\partial z^2}\right)=s(x,y,z),\quad (x,y,z)\in\Omega, \tag{1}$$

$$\phi(x,y,z)=\text{constant},\quad (x,y,z)\in\partial\Omega \tag{2}$$

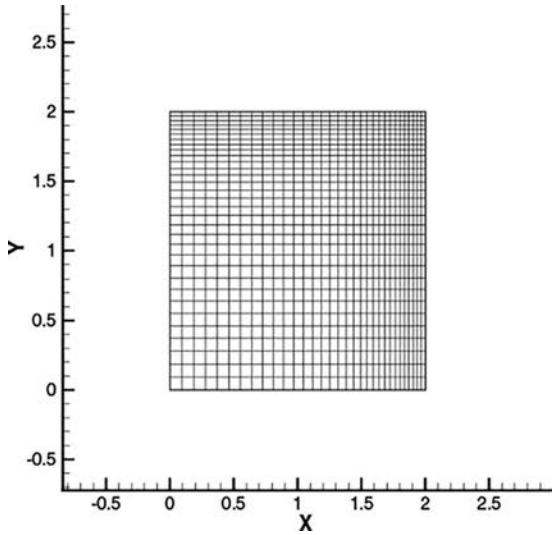

Figure 1. Nonuniform grid illustration in an *x-y* plane, n_x=n_y=30, λ_x=λ_y=0.5.

where Ω is a rectangular domain ($(x, y, z)\in[0, 2]\times[0, 2\eta]\times[0, 2]$) and $\partial\Omega$ is the boundary of the domain. The source function $s(x, y, z)$ and the solution variable $\phi(x, y, z)$ are smooth and differentiable. In the present paper, a source term of following form:

$$s(x,y,z) = -\left(2+\frac{\varepsilon}{\eta^2}\right)\pi^2 \sin\left(\frac{\pi}{\eta}y\right)\sin(\pi x)\sin(\pi z) \tag{3}$$

is assumed. Then, for the boundary condition of $\phi(x,y,z)$=0 following analytical solution of Eq. (1) can be obtained:

$$\phi(x,y,z) = \sin\left(\frac{\pi}{\eta}y\right)\sin(\pi x)\sin(\pi z) \tag{4}$$

This analytical solution will be used to compare the accuracy of difference schemes.

Cell-centered grids in which the grid points are placed at the centers of the cells are used in this paper. We divide the computed domain Ω into sub-intervals by the points $0 = x_0, x_1, \ldots, x_{n_x-1}, x_{n_x} = 2$, $0 = z_0, z_1, \ldots, z_{n_z-1}, z_{n_z} = 2$, and $0 = y_0, y_1, \ldots, y_{n_y-1}, y_{n_y} = 2\eta$. Nonuniform grid is used by the following stretching function:

$$x_i = 2\times\left[\frac{i}{n_x}+\frac{\lambda_x}{n_x}\cdot\sin\left(\frac{\pi\cdot i}{n_x}\right)\right], \quad 0\le i\le n_x \tag{5a}$$

$$z_k = 2\times\left[\frac{i}{n_z}+\frac{\lambda_z}{n_z}\cdot\sin\left(\frac{\pi\cdot k}{n_z}\right)\right], \quad 0\le k\le n_z \tag{5b}$$

$$y_j = 2\eta\times\left[\frac{i}{n_y}+\frac{\lambda_y}{n_y}\cdot\sin\left(\frac{\pi\cdot j}{n_y}\right)\right], \quad 0\le j\le n_y \tag{5c}$$

Parameters λ_x, λ_y, and λ_z are used to control grid clustering (Figure 1 for illustration). Its absolute value ranges from -1 to 1 and grids are tuned to be uniform when λ_x=λ_y=λ_z=0.

The forward and backward difference step lengths are, respectively, defined by x_f=x_{i+1}−x_i and x_b=x_i−x_{i-1} in the x-direction. And similarly, y_f, y_b, z_f, z_b can be defined (Figure 2). Kalita et al. [13] proposed a transformation-free HOC scheme for the steady 2D convection–diffusion equation on nonuniform gird. Following the same procedure, by means of Taylor series expansion, HOC

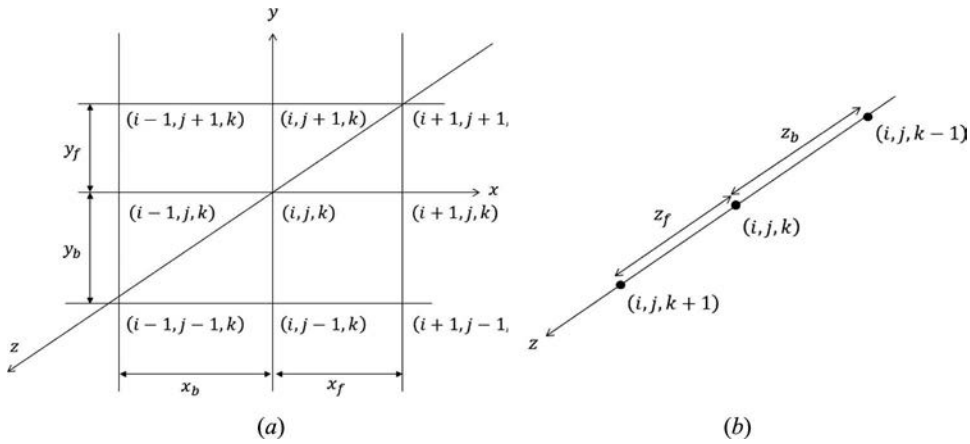

Figure 2. Nonuniform grid compact scheme stencil: (a) *x-y* plane; (b) z direction.

scheme on nonuniform grids for the 3D anisotropy diffusion equation, Eq. (1), is written as

$$\begin{aligned}&\Big[\delta_x^2+\delta_z^2+\varepsilon\delta_y^2+H_x\delta_x\left(\delta_z^2+\varepsilon\delta_y^2\right)+H_z\delta_z\left(\delta_x^2+\varepsilon\delta_y^2\right)\\&+H_y\delta_y\left(\delta_x^2+\delta_z^2\right)+(K_x+K_z)\delta_x^2\delta_z^2+\left(\varepsilon K_x+K_y\right)\delta_x^2\delta_y^2+\left(\varepsilon K_z+K_y\right)\delta_y^2\delta_z^2\Big]\phi_{i,j,k}=S_{i,j,k}\end{aligned} \tag{6}$$

where H, K, and S are given by

$$H_x=\frac{1}{3}\left(x_f-x_b\right),\quad H_y=\frac{1}{3}\left(y_f-y_b\right),\quad H_z=\frac{1}{3}\left(z_f-z_b\right) \tag{7a}$$

$$\begin{aligned}K_x&=\frac{1}{12}\left(x_b^2+x_f^2-x_bx_f\right),\quad K_y=\frac{1}{12}\left(y_b^2+y_f^2-y_by_f\right),\\K_z&=\frac{1}{12}\left(z_b^2+z_f^2-z_bz_f\right)\end{aligned} \tag{7b}$$

and

$$S_{i,j,k}=\left[1+H_x\delta_x+H_z\delta_z+H_y\delta_y+\left(K_x-1.5H_x^2\right)\delta_x^2+\left(K_y-1.5H_y^2\right)\delta_y^2+\left(K_z-1.5H_z^2\right)\delta_z^2\right]s_{i,j,k} \tag{7c}$$

In the x-direction, finite difference operators δ_x and δ_x^2 are defined by

$$\begin{aligned}\delta_x\phi_{i,j,k}&=\frac{\phi_{i+1,j,k}-\phi_{i-1,j,k}}{x_f+x_b},\\\delta_x^2\phi_{i,j,k}&=\frac{2}{\left(x_f+x_b\right)}\left[\frac{\phi_{i-1,j,k}}{x_b}+\frac{\phi_{i+1,j,k}}{x_f}-\left(\frac{1}{x_b}+\frac{1}{x_f}\right)\phi_{i,j,k}\right]\end{aligned} \tag{8}$$

Finite difference operators in the y- and z-direction can be defined similarly.

For convenient expression, first- and second-order difference operator δ_x and δ_x^2 can be rewritten as

$$\begin{aligned}\delta_x\phi_{i,j,k}&=L_x\phi_{i-1,j,k}+R_x\phi_{i+1,j,k},\\\delta_x^2\phi_{i,j,k}&=A_x\phi_{i-1,j,k}+B_x\phi_{i,j,k}+C_x\phi_{i+1,j,k}\end{aligned} \tag{9}$$

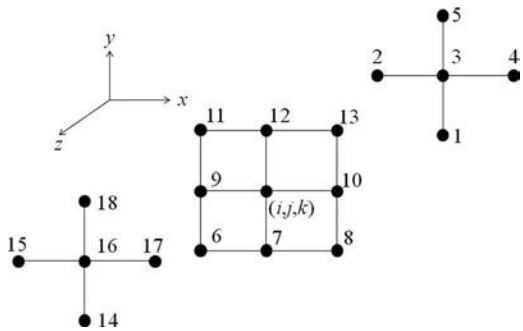

Figure 3. Grid points labeling of the 19-point HOC difference scheme stencil.

$$L_x = -\frac{1}{x_b + x_f}, \quad R_x = \frac{1}{x_b + x_f}, \quad A_x = \frac{2}{(x_b + x_f)x_b},$$
$$B_x = -\frac{2}{x_b x_f}, \quad C_x = \frac{2}{(x_b + x_f)x_f} \tag{10}$$

Similarly, δ_y, δ_y^2 and δ_z, δ_z^2 can be defined.

Substituting operator formulas Eq. (8) into Eq. (6), considering node numbering shown in Figure 3, 19 points HOC scheme for the 3D anisotropy diffusion equation, Eq. (1), on nonuniform grids can be derived as follows:

$$\sum_{nb=1\sim 18} a_{nb}\phi_{nb} - a_p\phi_{i,j,k} = rhs_{i,j,k} \tag{11}$$

The coefficients $a_{nb}(nb{=}1\sim 18)$, a_p, and $rhs_{i,\ j,\ k}$ are given as:

$$a_1 = H_y L_y A_z + \varepsilon H_z L_z A_y + (K_y + \varepsilon K_z) A_y A_z,$$

$$a_2 = H_x L_x A_z + H_z L_z A_x + (K_x + K_z) A_x A_z,$$

$$a_3 = A_z + H_z L_z (B_x + \varepsilon B_y) + (K_x + K_z) B_x A_z + (K_y + \varepsilon K_z) B_y A_z,$$

$$a_4 = H_x R_x A_z + H_z L_z C_x + (K_x + K_z) C_x A_z,$$

$$a_5 = H_y R_y A_z + \varepsilon H_z L_z C_y + (K_y + \varepsilon K_z) C_y A_z,$$

$$a_6 = \varepsilon H_x L_x A_y + H_y L_y A_x + (\varepsilon K_x + K_y) A_x A_y,$$

$$a_7 = \varepsilon A_y + H_y L_y (B_x + B_z) + (\varepsilon K_x + K_y) B_x A_y + (K_y + \varepsilon K_z) A_y B_z,$$

$$a_8 = \varepsilon H_x R_x A_y + H_y L_y C_x + (K_y + \varepsilon K_x) C_x A_y,$$

$$a_9 = A_x + H_x L_x (B_z + \varepsilon B_y) + (K_y + \varepsilon K_x) A_x B_y + (K_x + K_z) A_x B_z,$$

$$a_{10} = C_x + H_x R_x (B_z + \varepsilon B_y) + (K_y + \varepsilon K_x) C_x B_y + (K_x + K_z) C_x B_z,$$

$$a_{11} = \varepsilon H_x L_x C_y + H_y R_y A_x + \left(K_y + \varepsilon K_x\right) C_y A_x,$$

$$a_{12} = \varepsilon C_y + H_y R_y (B_x + B_z) + \left(\varepsilon K_x + K_y\right) B_x C_y + \left(K_y + \varepsilon K_z\right) C_y B_z,$$

$$a_{13} = \varepsilon H_x R_x C_y + H_y R_y C_x + \left(K_y + \varepsilon K_x\right) C_y C_x,$$

$$a_{14} = H_y L_y C_z + \varepsilon H_z R_z A_y + \left(K_y + \varepsilon K_z\right) A_y C_z,$$

$$a_{15} = H_x L_x C_z + H_z R_z A_x + (K_x + K_z) A_x C_z,$$

$$a_{16} = C_z + H_z R_z \left(B_x + \varepsilon B_y\right) + (K_z + K_x) C_z B_x + (K_x + \varepsilon K_z) C_z B_y,$$

$$a_{17} = H_x R_x C_z + H_z R_z C_x + (K_z + K_x) C_z C_x,$$

$$a_{18} = H_y R_y C_z + \varepsilon H_z R_z C_y + \left(K_y + \varepsilon K_z\right) C_y C_z,$$

$$\begin{aligned} a_p &= B_x + B_z + \varepsilon B_y + \left(\varepsilon K_x + K_y\right) B_x B_y + \left(K_y + \varepsilon K_z\right) B_y B_z + (K_x + K_z) B_x B_z \\ rhs_{i,j,k} &= \left[H_x L_x + \left(K_x - 1.5 H_x^2\right) A_x\right] s_{i-1,j,k} + \left[H_x R_x + \left(K_x - 1.5 H_x^2\right) C_x\right] s_{i+1,j,k} \\ &+ \left[H_y L_y + \left(K_y - 1.5 H_y^2\right) A_y\right] s_{i,j-1,k} + \left[H_y R_y + \left(K_y - 1.5 H_y^2\right) C_y\right] s_{i,j+1,k} \\ &+ \left[H_z L_z + \left(K_z - 1.5 H_z^2\right) A_z\right] s_{i,j,k-1} + \left[H_z R_z + \left(K_z - 1.5 H_z^2\right) C_z\right] s_{i,j,k+1} \\ &+ \left[1 + \left(K_x - 1.5 H_x^2\right) B_x + \left(K_y - 1.5 H_y^2\right) B_y + \left(K_z - 1.5 H_z^2\right) B_y\right] s_{i,j,k}. \end{aligned} \tag{12}$$

3. Parallel scalable MG method

Multigrid method as a well-known and most efficient algorithm has been widely applied to solve the discretized elliptic partial differential equations. MG algorithms include four basic components: restriction, prolongation, relaxation operator, and cycling method. Unlike other iterative methods, the convergence speed of MG method is independent of the discretization mesh size [16,17]. A geometry parallel MG method on cell-centered grids is adopted in the present paper. With the aid of message passing interface (MPI) library [18], an MG program can run on multiple cores under the context of a distributed memory environment. To achieve scalability and good parallel performance, each component of MG needs to be chosen carefully. In the following section, MG components and corresponding parallelism will be discussed.

Grid partitioning is a natural choice of geometric MG approach and one-dimensional (1D) spatial partitioning is employed in the present study. For a 3D problem, the dimension of communication messages between processors is two. MG is intrinsically hard to parallel in comparison with other iterative algorithms because of that data-parallelism is different on every grid levels. The ratio of communication to the computing time decreases as grids become coarser. The problem of the communication overhead at the coarsest grid needs to be treated carefully. At the coarsest grid, when number of grids is lower than number of processors, only one processor is responsible for the computation and other processors remain idle. Figure 4 exemplifies a 1D grid partitioning for four processors. When grid level goes down to the coarsest, the number of grids is only half of the number of processors. As a result, three processors keep idle at the coarsest grid level. A parallel V cycle has advantage over W and other parallel cycles because less often the coarse girds are processed in one MG cycle. Then, V cycle is adopted in the present MG algorithm.

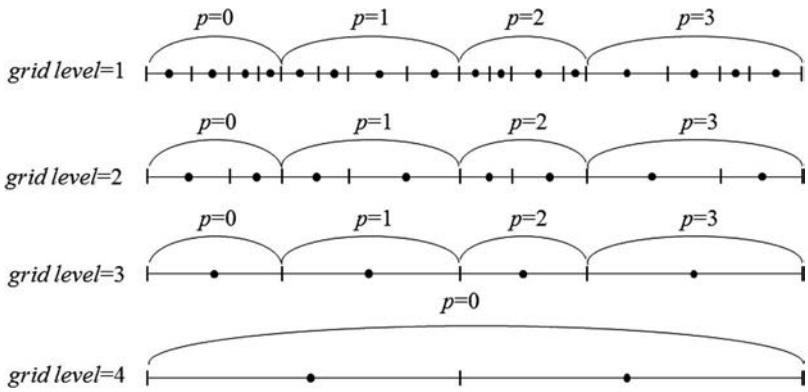

Figure 4. Grids partitioned for four processors and corresponding to 16 finest grid points.

Restriction operators are used to transfer residuals on fine grids to coarse grids. For cell-centered discretization, eight-point average restriction operator is frequently used to calculate the residuals on coarse grids. To evaluate the residuals with more accuracy on coarse grids, a volume weighting eight-point average restriction operator is adopted on nonuniform grids. Figure 5 shows the restriction operators on nonuniform grids in the context of different coarsening strategies. $R_{i,\ j,\ k}$ is residual at coarse grid point (i, j, k) and $r_n(n{=}1 \sim 8)$ are corresponding fine grid points residuals. $V_{i,\ j,\ k}$ represents grid volume at coarse grid point and $v_n(n{=}1 \sim 8)$ is grid volume at fine grid points. It is to be noticed that the closer the distance from fine grid point to coarse grid point (with small volume), the more contributions to the residuals. So the weighting coefficient is given by v_n/V, and this idea is similar to the area law for 2D MG method [19]. The weighting restriction operator on nonuniform grids for different choices of coarse grids can be calculated as following:

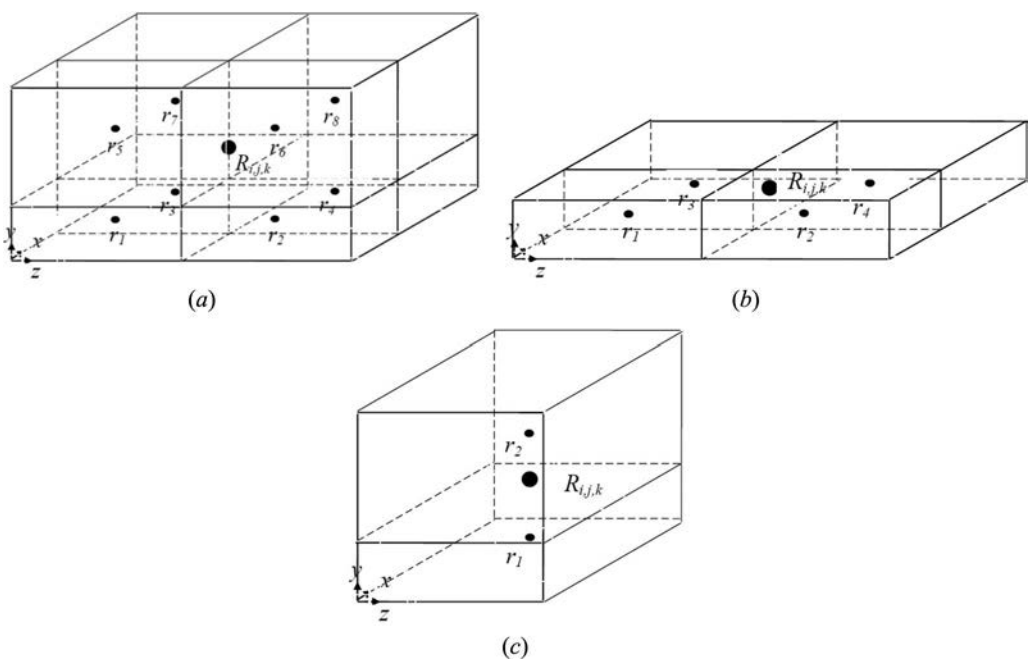

Figure 5. Schematic diagram of a restriction operator on nonuniform grids: (*a*) standard coarsening; (*b*) 2D semi-coarsening; and (*c*) 1D semi-coarsening.

$$\text{Figure 5(a) standard coarsening}: \; R_{i,j,k} = \frac{1}{V}\sum_{n=1}^{8} v_n r_n \tag{13a}$$

$$\text{Figure 5(b) 2D semi-coarsening}: \; R_{i,j,k} = \frac{1}{V}\sum_{n=1}^{4} v_n r_n \tag{13b}$$

$$\text{Figure 5(c) 1D semi-coarsening}: \; R_{i,j,k} = \frac{1}{V}\sum_{n=1}^{2} v_n r_n \tag{13c}$$

Restriction calculations at different grids are independent of each other; even message communication is not needed except the coarsest grid level in Figure 4.

Prolongation operators are used to interpolate residuals from coarse grids to fine grids. Trilinear prolongation (TP) is used for standard coarsening MG. Bilinear prolongation (BP) and linear prolongation (LP) are used for 2D semi-coarsening and 1D semi-coarsening MG, respectively. Prolongation calculations at different grid points are also independent of each other; but unlike restriction operators, message communication is needed. Compared with constant prolongation operator that simply assigns the values of coarse grids to the corresponding fine grids (i.e., direct injection), present prolongation operators are more accurate and they can reduce the numbers of MG iterations drastically. Section 4.3 will give a result for example.

Relaxation operators are the crucial MG component with regard to parallelism. Under different circumstances, four colors point-successive over relaxation (SOR) and line-SOR are adopted in MG algorithm. The colored point-SOR relaxation is easy to parallel since the grids with each color can be updated independently. Line-SOR relaxation needs to solve a linear tridiagonal equation (TDE) within each relaxation. Divide and conquer (DAC) algorithm is very useful to solve TDE on parallel computers because of high efficiency and flexibility [20], so it is adopted in this paper. The details of the DAC algorithm can be referred to paper [20].

All programs are running on the SUGON cluster of our research group [21]. SUGON consists of 32 compute nodes; for each node, there are 16 cores 2.6GHz central processing unit (CPU) and 32 GB RAM.

4. Numerical results

4.1. Accuracy comparison

At first, HOC difference scheme accuracy on nonuniform grids is compared with standard central difference scheme. The analytical solution of Eq. (1) ($\varepsilon=\eta=1$) is taken as the reference. Uniform girds and a nonuniform with $\lambda_x = 0.5$, $\lambda_y = -0.5$, $\lambda_z = 0.3$ are adopted. All multigrid iterative procedures are terminated by stopping criterion 2 of [22], that is, $\|\vec{r}\| \le stop\_tol \cdot \left\|rhs_{i,j,k}\right\|$, where $\|\vec{r}\|$ is the Euclidean norm (two-norm) of the residual vector and $stop\_tol$ is 10^{-10}. Convergence rate M is calculated as [13]

$$M = \frac{\log(e_1/e_2)}{\log(N_2/N_1)} \tag{14}$$

where e_1 and e_2 are the absolute maximum errors estimated for two different grids with N_1 and N_2 grid points.

Table 1 compares the absolute maximum errors on different grids for two difference schemes. It is obvious that convergence rate of HOC difference scheme is greater than or a least equal to 4 regardless of grid stretching. Errors of HOC scheme are smaller than that of standard central difference scheme with the same grid size. Also from Table 1, we can see that absolute maximum errors are increasing when grid is stretched for all difference schemes.

Table 1. Comparison of errors on uniform and nonuniform grids, η=ε = 1.

Grid			Uniform grids				Nonuniform grids			
			Standard central scheme		HOC compact scheme		Standard central scheme		HOC compact scheme	
n_x	n_y	n_z	Error	Rate	Error	Rate	Error	Rate	Error	Rate
16	8	10	2.98×10^{-2}		3.75×10^{-3}		5.86×10^{-2}		1.53×10^{-2}	
32	16	20	7.84×10^{-3}	1.93	1.62×10^{-4}	4.53	1.58×10^{-2}	1.89	9.49×10^{-4}	4.01
64	32	40	2.01×10^{-3}	1.96	8.02×10^{-6}	4.34	3.92×10^{-3}	2.01	3.89×10^{-5}	4.61

Table 2. Comparison of errors on uniform grids with $\varepsilon=10^3$ and η=0.1.

Grid				
n_x	n_y	n_z	Error	Rate
16	8	10	1.04×10^{-1}	
32	16	20	1.33×10^{-2}	2.97
64	32	40	1.88×10^{-3}	2.82

And then taking the analytical solution of Eq. (1) as the references with $\varepsilon = 10^3$ and $\eta = 0.1$, $\lambda_x = \lambda_y = \lambda_z = 0$, in which anisotropy is caused by large coefficient in y-direction. Table 2 gives errors obtained from the HOC difference schemes for different grid sizes. As shown in the table, the rate of convergence is nearly equal to 3 which is still better than standard central difference scheme.

4.2. Parallel performance comparison

Parallel performance of the HOC scheme is compared with standard central difference scheme in this section. We choose ε=η=1 and n_x=64, n_y=128, n_z=32 in Eq. (1). A multigrid $V(3,1)$ cycle is adopted in both schemes and also the same restriction and prolongation operators and the same convergence criterion are used. For the 19-point HOC scheme, four-color SOR relaxation can decouple the grids completely [13]. And for the 7-point central difference scheme, only the red-black two-color SOR relaxation is needed to parallelize. To achieve a good efficiency on a parallel computer, the ratio between computation time t_{comp} and communication time t_{comm} should be large. The number of communication messages of the HOC scheme is two times of the second-order central difference scheme. At the meantime, in one iteration, operators of 19-points HOC scheme are nearly three times as much as 7-point central difference scheme [10]. Figure 6 displays the relationship between the number of cores and speed up S_p, and the relationship between the number of cores and parallel

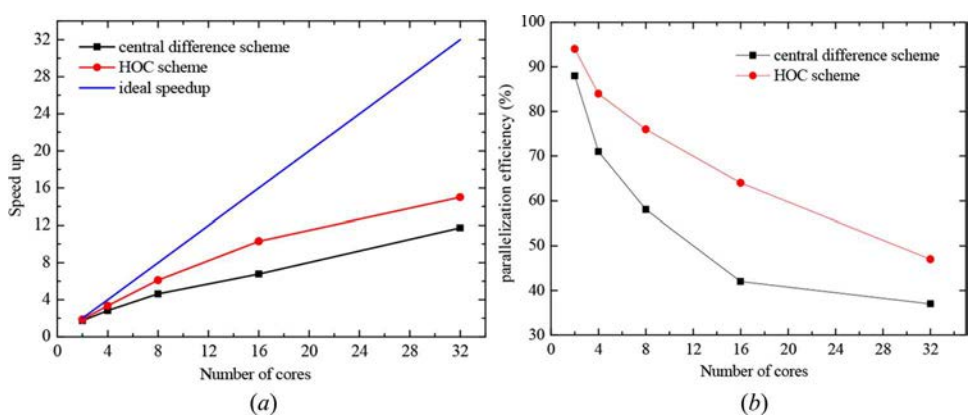

Figure 6. Comparison of the parallel performance of two different schemes: (*a*) numbers of cores vs. speed up; (*b*) numbers of cores vs. parallelization efficiency.

Table 3. The CPU time in seconds with two different difference schemes.

Number of cores	CPU time (s)	
	Central difference scheme	HOC difference scheme
1	0.88	1.65
2	0.50	0.88
4	0.31	0.49
8	0.19	0.27
16	0.13	0.16
32	0.08	0.11

HOC, high-order compact.

efficiency E_p, defined by

$$S_p = \frac{T(1)}{T(p)} \tag{15}$$

$$E_p = \frac{S_p}{p} \times 100\% \tag{16}$$

where $T(p)$ is computing time for a given problem which runs on p cores. The HOC difference scheme with MG shows noticeably better parallel performance than central difference scheme with MG. Table 3 gives the CPU time in seconds with two different difference schemes, the HOC difference scheme takes up more time owing to more iteration per grid point. In the following, two special cases will be studied in detail with different parameters of ε and η.

4.3. Case 1

Consider Eq. (1) with $\varepsilon=10^{-3}$ and $\eta=2$. If Eq. (1) is used to solve heat conduction in solid, then ε is the coefficient of thermal conductivity. $\varepsilon=10^{-3}$ means thermal resistance is very large in the y-direction. Variable Φ changes faster in the x- and z-directions, and slower in the y-direction. Then, grid numbers are set to $n_x=256$, $n_z=512$, and $n_y=32$. In this case, it cannot be treated efficiently with pointwise relaxation and standard coarsening. The reason is that pointwise relaxation performances badly in the non-dominant direction, that is, in the y-direction. Semi-coarsening in the x- and z-directions, combined with four-color relaxation, is appropriate for the present case. MG grid levels were 8 and then the coarsest grid is 4×8×32. Started with zero initial guess, computation will converge in 20 MG $V(2,1)$ iterations when *stop_tol* is reduced by 10^{-10}. Figure 7 shows the variation of

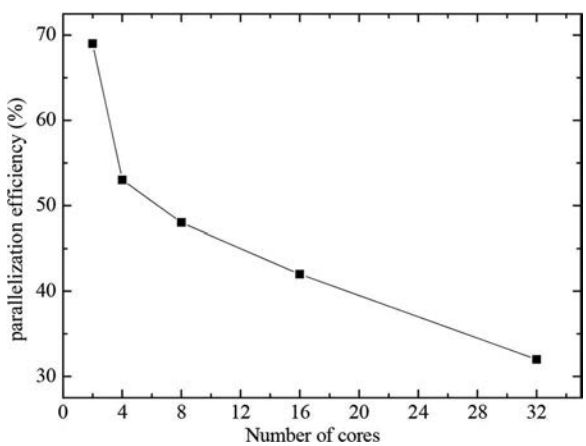

Figure 7. Numbers of cores vs. parallelization efficiency for case 1.

Table 4. Number of iterations and the CPU time in seconds for case 1.

Point-SOR		Alternation line-SOR		MG with standard coasening		MG with semi-coarsening in the *x*- and *z*-directions	
Iteration	CPU	Iteration	CPU	Iteration	CPU	Iteration	CPU
Not converged		1,788	2,092	17,536	10,408	20	17.4

SOR, successive over relaxation; MG, multigrid.

parallelization efficiency along with numbers of cores. It can be seen that as the numbers of cores increases, parallelization efficiency decreases. For the numbers of cores ranging from 2 to 32, the corresponding parallelization efficiency decreases from 69 to 32%.

Table 4 gives the comparison between MG with semi-coarsening strategy and other methods. The maximum number of iterations is set to 20,000. Point-SOR iteration (relaxation factor is 1.5) is not converged. CPU time cost of MG with standard coarsening is 10,408s, that is much higher than alternation line-SOR iteration (2,092s) and tremendously higher than MG with semi-coarsening in the *x*- and *z*-directions (17.4s). Failure and inferior of standard coarsening and point-SOR relaxation are obvious.

In addition, accuracy of prolongation operator will have a strong influence on MG algorithm convergence. If constant prolongation operator is adopted in the present case, the CPU cost of a single core is 60.5s, which is more than three times as CPU cost as bilinear prolongation (17.4s).

4.4. Case 2

Consider Eq. (1) with $\varepsilon=10^3$ and $\eta=2$. In the present case, it has a strong coupling of variable Φ in the *y*-direction. To get an accurate resolution of variable Φ, we set larger numbers of grids in the regions of larger gradients, that is, $n_y=512$, $n_x=64$, and $n_z=32$. Semi-coarsening in *y*-direction along with line-SOR relaxation in the *y*-direction is adopted in the present computation. Line-SOR relaxation is parallelled by DAC method. MG grid levels were 6 and the coarsest grid is $16\times64\times32$. The variation of parallelization efficiency with respect to numbers of cores is presented in Figure 8. In the present case, the amount of massage communication is constant in all the grid levels. Then, the ratio between t_{comp} and t_{comm} drastically decreases as MG levels go down to the coarsest grid. From Figure 8, parallelization efficiency decreases from 91 to 23% as numbers of cores increases. Table 5 shows that the cost of CPU time varies with CPU cores. From Table 5, it can be observed that the present MG algorithm is still scalable although parallel efficiency is very low at 32 CPU cores (about 25% as shown in Figure 8).

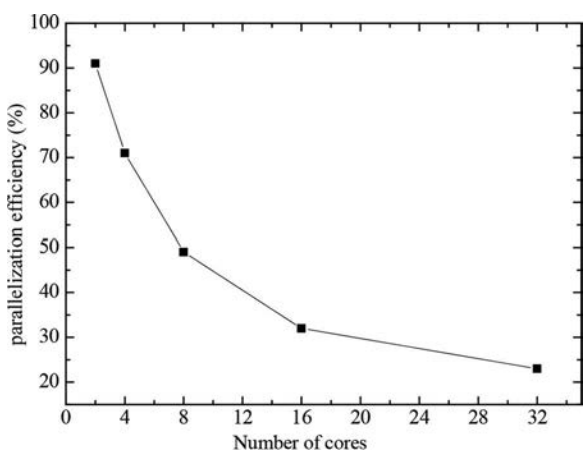

Figure 8. Numbers of cores vs. parallelization efficiency for case 2.

Table 5. The CPU time in seconds for case 2.

Number of cores	CPU time (s)
1	5.12
2	2.81
4	1.80
8	1.30
16	1.00
32	0.70

5. Conclusion

The objective of this paper is to develop a multigrid algorithm to solve anisotropy elliptic diffusion problems. MG components on nonuniform grids and corresponding parallelism characteristics are discussed. Different semi-coarsening strategies and relaxation operators are adopted for diverse anisotropy applications. Numerical results show that MG method combined with the HOC difference scheme is very accurate and efficient, and easy to parallelize by the aid of MPI.

Funding

This work has been supported by the National Natural Science Foundation of China (Grant numbers 51136004) and the Key Project of International Joint Research of NSFC (51320105004). The computational sources of China Grid of Energy of Key Laboratory of Thermo-Fluid Science and Engineering are greatly acknowledged.

References

[1] From wikipedia: https://en.wikipedia.org/wiki/Anisotropy.
[2] S. M. Grove, Anisotropy of Heat Conduction in Fibre-Reinforced Composites, Ph.D. thesis, University of Plymouth, 1985.
[3] Y. Ge, and F. Cao, Multigrid Method Based on the Transformation-Free HOC Scheme on Nonuniform Grids for 2D Convection Diffusion Problems, *J. Comput. Phys.*, vol. 230, pp. 4051–4070, 2011.
[4] S. K. Dekema, and D. H. Schultz, High-order Methods for Differential Equation with Large First-Derivative terms, *Int. J. Numer. Methods Fluids.*, vol. 10, pp. 259–284, 1990.
[5] X. Y. Wang, H. Qi, S. G. Wang, and L. M. Ruan, The Combined Radiative Integral Equations and Finite-Element Method for Radiation in Anisotropic Scattering Media, *Numer. Heat Transfer B Fund.*, vol. 61, no. 5, pp. 387–411, 2012.
[6] B. Hunter, and Z. Guo, Comparison of Quadrature Schemes in DOM for Anisotropic Scattering Radiative Transfer Analysis, *Numer. Heat Transfer B Fund.* vol. 63, no. 6, pp. 485–507, 2013.
[7] T. W. Tsai, Y. M. Lee, and Y. C. Shiah, Heat Conduction Analysis in Thin Film Irradiated by an Ultrafast Pulse Laser Heating, *Numer. Heat Transfer A Appl.*, vol. 64, no. 2, pp. 132–152, 2013.
[8] K. Guedri, A. S. Al-Ghamdi, A. Bouzid, M. A. Abbassi, and H. A. Ghulman, Evaluation of the FTn Finite Volume Method for Transient Radiative Transfer in Anisotropic Scattering Medium, *Numer. Heat Transfer A Appl.*, vol. 68, no. 10, pp. 1137–1154, 2015.
[9] X. Liu, P. Ming, W. Zhang, L. Fu, and L. Jing, Finite-Volume Methods for Anisotropic Diffusion Problems on Skewed Meshes, *Numer. Heat Transfer B Fund.* vol. 68, no. 3, pp. 239–256, 2015.
[10] M. M. Gupta, and J. Zhang, High Accuracy Multigrid Solution of the 3D Convection-Diffusion Equation, *Appl. Math. Comput.*, vol. 113, pp. 249–274, 2000.
[11] J. Zhang, L. Ge, and J. Kouatchou, A Two Colorable Fourth-Order Compact Difference Scheme and Parallel Iterative Solution of the 3D Convection Diffusion Equation, *Math. Comput. Simulat.*, vol. 54, pp. 65–80, 2000.
[12] Y. Wang, and J. Zhang, Sixth Order Compact Scheme Combined with Multigrid Method and Extrapolation Technique for 2D Poission Equation, *J. Comput. Phys.*, vol. 228, pp. 137–146, 2009.
[13] J. C. Kalita, A. K. Dass, and D. C. Dalal, A Transformation-free HOC Scheme for Steady Convection-Diffusion on Non-uniform Grids, *Int. J. Numer. Meth. Fluids.*, vol. 44, pp. 33–53, 2004.
[14] Y. Ge, and F. Cao, Multigrid Method Based on the Transformation-Free HOC Scheme on Nonuniform Grids for 2D Convection Diffusion Problems, *J. Comput. Phys.*, vol. 230, pp. 4051–4070, 2011.
[15] M. Prieto, R. Santiago, D. Espadas, I. M. Liorente, and F. Tirado, Parallel Multigrid for Anisotropic Elliptic Equations, *J. Parallel. Dis. Comput.*, vol. 61, pp. 96–114, 2001.
[16] P. Wesseling, *An Introduciton to Multigrid Methods*, Wiley, Chichester, 1992.
[17] W. Q. Tao, *Numerical Heat Transfer*, Xi'an Jiaotong University Press, Xi'an, 2001.

[18] W. Gropp, E. Lusk, N. Doss, and A. Skjellum, A High-Performance, Portable Implementation of the MPI Message Passing Interface Standard, *Parallel Comput.*, vol. 22, pp. 789–828, 1996.
[19] C. Liu, Multilevel Adaptive Methods in Computational Fluid Dynamics, Ph.D. thesis, Universtity of Colorado at Denver, 1989.
[20] S. Bondeli, Divide and Conquer: A New Parallel Algorithm for the Solution of a Tridiagonal Linear System of Equations, *Parallel Comput.*, vol. 17, pp. 419–434, 1991.
[21] L. Chen, Y. L. He, and W. Q. Tao, The Temperature Effect on the Diffusion Processes of Water and Proton in the Proton Exchange Membrane Using Molecular Dynamics Simulation, *Numer. Heat Transfer A Appl.*, vol. 65, no. 3, pp. 216–228, 2013.
[22] R. Barrett, M. Berry, T. F. Chan, J. Demmel, J. Donato, J. Dongarra, V. Eijkhout, R. Pozo, C. Romine, and H. van der Vorst, *Templates for the Solution of Linear Systems: Building Blocks for Iterative Methods*, 2nd ed., Society for industrial and Applied Mathematics, Philadelphia, PA, 2010.